MEKATRONIKA
JOURNAL OF MECHATRONICS AND INTELLIGENT MANUFACTURING
E-ISSN: 2637-0883
VOLUME 6, ISSUE 2, JULY, 2024, 96 – 111
DOI: https://doi.org/10.15282/mekatronika.v6i2.10801

RESEARCH ARTICLE

Numerical Model Validation of Cyclone Separator with Square Cross-sectional Vortex Finder for Oil Palm Loose Fruit Collection

Adam Danial Lim Jefri Lim[1,4], Saiful Anuar Abu Bakar[1,3], Mohd Faridh Ahmad Zaharuddin[2] and Mohd Farid Muhamad Said [3]

[1]Department of Aeronautics, Automotive and Ocean Engineering, Faculty of Mechanical Engineering, Universiti Teknologi Malaysia, 81310 Skudai, Johor, Malaysia.
[2]Department of Manufacturing and Industrial Engineering, Faculty of Mechanical Engineering, Universiti Teknologi Malaysia, 81310, Skudai, Johor, Malaysia
[3]Automotive Development Centre, Institute of Vehicle Systems and Engineering, Universiti Teknologi Malaysia, 81310, Skudai, Johor, Malaysia
[4]Department of Agricultural and Biosystems Engineering, Faculty of Engineering, Universiti Putra Malaysia, 43400, Serdang, Selangor, Malaysia.

ABSTRACT - Cyclone separators are commonly employed in the industry for material separation because of their practicality. For the exact reason, the technology was expanded to harvest oil palm loose fruits. However, there is a scarcity of data in the utilization of computational fluid dynamics (CFD) in the field. Hence, a numerical model validation is essential in determining the model accuracy in representing flow of cyclone separators Consequently, the current study aims to validate the numerical model with experimental data on factors such as pressure drop, tangential velocity and axial velocity. Results indicate that the model behaves at a satisfactory level with minor errors. Upon successfully validating the numerical model, Reynold's Stress Model (RSM) and Discreet Phase Model (DPM) were used to simulate an oil palm loose fruit collecting system where density 995.7 kg/m^3 and size 0.04 m was set to simulate oil palm loose fruits in the system. Turbulence intensity at the gas and particles outlet are specified at 5%. It was found that Rankine vortex was present in the system, confirming the working principal of the cyclone separator. Further optimization works was conducted by modifying the cyclone's separator configuration to a square vortex finder where a collection efficiency of 92.08 % was recorded.

ARTICLE HISTORY
Received : 4th June 2024
Revised : 3rd Oct 2024
Accepted : 25th Dec 2024
Published : 30th Dec 2024

KEYWORDS
Computational fluid dynamics
Cyclone separator
Discrete phase model
Oil palm loose fruit
Reynold's stress model

1.0 INTRODUCTION

In oil palm loose fruit collection, the most preferable method of collection is using the vacuum suction to obtain a high collection rate as opposed to manual method and roller loose fruit collector. However, in reality the industry still opted the manual method over the designed machines mainly due to design problems. Thus, it is essential to study and analyze the important parameters involved in the design process in ensuring an optimal design. In suction type oil palm loose fruit collector, an important parameter is the suction speed. A study was conducted by Khalid *et al*., [1] on the minimum suction speed required to operate the MK III, a pneumatic oil palm loose fruit collector designed by Shuib *et. al.*, [2] however this study is conducted based on the manipulation of the machine's throttle condition and is therefore specific to the air velocity only. No other study on suction mechanism on oil palm loose fruits is found. Therefore, a detailed study on the parameters involved in the loose fruit collection machine and the interactions between the parameters is essential.

Currently, one of the most opted methods of separation in the industry is using the cyclonic separator where it offers a variety of benefits. The design of cyclone separators is generally simple with minimal maintenance and variable working temperature, which is a main reason it is opted by the industry as a method for material separation. According to Park and Go, [3], the working principle of the air cyclone separator is as materials are being sucked in through the inlet, a centrifugal force will act on the materials which forces them to the separator walls while the drag force acting on the materials forces them to the centre of the cyclone separator. Thus, heavy or course materials will remain on the walls, swirling down to be collected via the outer vortex of the cyclone separator while lighter fine materials that has been dragged to the centre of the cyclone where the inner vortex is located will be transported out of the system. Classical cyclonic separators, 1D3D, 1D2D and 2D2D are the usual designs to start with for designing, despite going back as far the 30s [4]. This is because the cyclone separators are relatively efficient and optimization efforts have also considered the design of the standard cyclones. Safikhani *et. al.*, [5], used Computational Fluid Dynamics (CFD) to numerically

***CORRESPONDING AUTHOR | Adam Danial Lim Jefri Lim** | ✉ adamdaniallim@graduate.utm.my

simulate the airflows in all three classical cyclone separator design. The researchers found that 1D3D is the most efficient in terms of particle separation. However, a recent study by El-Emam *et. al*., [6], whom studied the performance of 5 different cyclone separators mainly the three classical designs, a 1D3D cyclone with 2D2D inlet and a newly designed cyclone separator. The most efficient cyclone separator is found to be the 1D2D cyclone among the rest. Note that the study simulated the removal of bio-particulate matter and leaves during the collection of jojoba seeds. Hence, the 1D2D cyclone separator is a suitable design to be considered for oil palm loose fruit collection as backed by the recent study due to the similarity of the intended usage that is, to separate foreign materials from fruit collection.

Previous designs of cyclonic separators intended for oil palm loose fruits collections are reported to be unsatisfactory in terms of collection efficiency due to the capacity of fruits in the cyclonic vacuum chamber. One of the underlying causes are, the storage of materials in a cyclone will affect its working principle and thus affecting the cyclone efficiency. Among the working principle are the tangential velocity, radial velocity, axial velocity, pressure drop as studied using computational fluid dynamics (CFD) and reported by numerous literature [7-10]. A design of dual cyclonic vacuum is proposed in the study to separate debris from loose fruits efficiently. The proposed design is constituted of two cyclone separators attached in parallel. Where the first cyclone is designed to collect clean loose fruits while the second cyclonic separator is intended to collect debris and other particulate matters sucked in the system.

In designing a cyclonic separator, several design parameters had been studied extensively by researchers in order to produce optimal design for such separators. The design parameters being studied include the inlet, vortex finder, cylinder to cone ratio, material collection system, gas outlet and wall roughness of cyclones. With the help of CFD, numerous studies have been conducted to study the effects of varying the vortex, specifically on the flow and collection efficiency of a cyclone separator. Several researches [11-14] have studied on varying the diameter and length of the vortex finder and found that the variations significantly affect the performance of cyclone separators. On another note, Wasilewski *et al.,* [8], studied the effect of varying the divergence and convergence of the vortex finder while Fu *et al.,* [7], evaluated the effects of slotted vortex finders in standard cyclone separators. Yao *et al.,* [15] studied the effects of multi-stage inlet ducts of cyclone separator and found that two stage inlets as presented in this study has the best separation efficiency. On the other hand, Surahmanto *et al.,*[16] worked on varying types of cones best for material separation and found that the single cone has the best efficiency. Results of all the works show significant results for cyclone separators operation. In this study, firstly the numerical CFD model is verified. Upon model verification, the same settings and conditions for the CFD model were used to simulate a conventional model and an improved model with a square vortex finder, where the collection efficiencies were compared and discussed extensively.

2.0 METHODS AND MATERIAL

2.1 Numerical Model Selection

In performing computations using CFD, firstly a suitable model must be chosen to navigate the simulation. This step is crucial in order to generate accurate results in observing flow in the cyclone separator. The fact that the flow in a cyclone separator is rather complex and is turbulent also gives a variety of choices of turbulent models to choose from. Other turbulent flow selections available are the Reynold's Stress Model (RSM), Large Eddy Simulation (LES) Model, Detached Eddy Simulation (DES) Model and the k-ε model. Table 1 shows the summary of details on CFD simulations of cyclone separators.

Table 1. Summary of numerical study on cyclone separators

Reference	Model	Type(s) of study on cyclone separator	Particle
[17]	RSM	Effects of inlet cross-sectional shape variations on multi-inlet cyclone separator.	DPM
[6]	RSM	Standard cyclone separators performance evaluation	DEM
[18]	RSM	Study on double tandem nesting cyclone	DPM
[7]	RSM	Effect of new vortex finder on cyclone separator performance	DPM
[19]	RSM	Effects of inlet structures variations to internal air flow.	n.a.
[20]	RSM	Industrial cyclone separator performance evaluation	n.a.
[21]	RSM	Two-stage series cyclone performance	n.a.
[3]	RSM	Study on cyclone separator critical diameter design	DPM
[8]	LES	Variations on vortex finder length and diameter on square cyclone separator performance	DPM

[11]	RSM	Variations on vortex finder diameter and inlet dimensions on cyclone separator gas flow	n.a.
[22]	LES	Effect of cylinder-cone ratio to flow in cyclone separator	DPM
[23]	RSM	Multi inlet guide channel effects.	DPM
[9]	RSM	Axial and reverse flow cyclone separators performance analysis	DPM
[12]	RSM	Effects of varying convergence and divergence of vortex finder in cyclone separators	DPM
[24]	RSM	Experimental and numerical study of Stairmand cyclone separators: a comparison of the results of small-scale and large-scale cyclones	DPM
[10]	RSM	Inner cone effect on cyclone separator flow field	n.a.
[25]	RSM	Variations of vortex finder diameter to cyclone efficiency	DPM
[26]	RSM	Effects of inlet temperature variations on single and double inlet cyclone	DPM
[27]	LES	Inlet angle effect on helical-roof inlet cyclone's collection efficiency.	DPM
[28]	RSM	Variations on cone length effects on flow in cyclone separators	n.a.
[29]	RSM	Multicriteria optimization of cyclone in clinker burning system	DPM
[30]	LES	Inlet angle effect on helical-roof inlet cyclone's flow and pressure drop.	n.a.
[31]	RSM	Study on flow dynamics of fluidised bed boiler cyclone separator	n.a.
[32]	LES	Gas outlet variations effects on cyclone separator performance	DPM
[33]	RSM	Wall roughness and vortex finder length effect on cyclone separator	n.a.
[34]	RSM	Effects of varying cyclone length to performance	DPM
[13]	LES	Variations on cyclone separator inlet dimensions.	DPM
[14]	RSM	Study on cyclone separator exit pipe selection	DPM
[35]	RSM	Dust outlet geometry effect on cyclone separator performance	DPM
[36]	LES	Effects of cone tip diameter variations on cyclone separator performance	DPM
[37]	RSM	Effects of vortex finder diameter variations to cyclone flow field and performance	DPM
[5]	RSM	Flow fields in standard cyclone separators	n.a.
[38]	RSM	Effects of cone tip diameter variations on cyclone separator performance	DPM

*RSM = Reynold's Stress Model
*LES = Large Eddy Simulation
*DPM = Discrete Phase Model
*DEM = Discrete Element Model
*n.a. = not available

As can be seen in Table 1, the most commonly used model for cyclone separator numerical analysis is the RSM with some opted for LES. [7] & [16], has opted RSM over LES generally because it uses less computational time with satisfactory accurate results. Moreover a study conducted by Hoekstra [39], has numerically simulated and performed experimental validation on the cyclone separator using several turbulence model which are the RSM, k-ε model and RNG k-ε . It was found that only the RSM can succesfully characterise the flow of cyclones accurately. Hence, RSM is the most suitable model in simulating the dual cyclone separator loose fruit collector. In considering the particle injection, DPM is favoured by most of the literature but one, that uses DEM. The basis for the selection is explained by the Ansys Fluent Theory Guide [40], where DPM is suitable for tracking particle bearing flows in which the dispersion occupies a low volume fraction and where collisions between particles can be ignored. This particular condition has made DPM viable and satisfactory for numerical simulations, as the separation mechanism of particles in a cyclone separator follows the aforementioned condition.

2.2 RSM Model Descriptions

According to Ansys Fluent Theory Guide [40], RSM works in such a way that it approaches the Reynolds-averaged Navier-Stokes (RANS) equations by solving the Reynolds stresses' transport equations alongside a dissipation rate equation. The model approaches effects of streamline curvature, swirl, rotation and also rapid variations in strain rates thoroughly, making the model essential in simulating cyclone flows.

The Reynolds stresses' transport equation is given as such:

$$\frac{\partial}{\partial t}(\rho_f \overline{u'_\iota u'_J}) + C_{ij} = D_{T,ij} + D_{L,ij} + P_{ij} + G_{ij} + \phi_{ij} + \varepsilon_{ij} + F_{ij} + S_u \quad (1)$$

where $\frac{\partial}{\partial t}(\rho_f \overline{u'_\iota u'_J})$ is the unsolved part of the RANS equation in tensor form, while C_{ij} , $D_{T,ij}$, $D_{L,ij}$, P_{ij} , G_{ij} , ϕ_{ij} , ε_{ij} , F_{ij} , S_u are the terms for equations of convection, turbulent diffusion, molecular diffusion, stress production, buoyancy production, pressure strain, dissipation, system rotation production and user defined source respectively.

In short, RSM functions to model and compute the unsolved equation, $\frac{\partial}{\partial t}(\rho_f \overline{u'_\iota u'_J})$ as shown in Equation (1) by solving the transport and dissipation equations. In producing the RANS equation, Reynolds Averaging is applied on the Navier-Stokes equation, resulting in:

$$\frac{\partial \rho}{\partial t} + \frac{\partial}{\partial x_i}(\rho u_i) = 0 \quad (2)$$

and

$$\frac{\partial}{\partial t}(\rho u_i) + \frac{\partial}{\partial x_j}(\rho u_i u_j) = \frac{\partial \rho}{\partial x_i} + \frac{\partial}{\partial x_j}\left[\mu\left(\frac{\partial u_i}{\partial x_j} + \frac{\partial u_j}{\partial x_i} - \frac{2}{3}\delta_{ij}\frac{\partial u_l}{\partial x_l}\right)\right] \quad (3)$$

$$+\frac{\partial}{\partial t}(\rho_f \overline{u'_\iota u'_J}) \quad (4)$$

where equations (2) and (3) are the RANS equations while equation (4) is the resulting effects of turbulence to be solved by RSM.

Turbulent Diffusion, $D_{T,ij}$

Going deeper on how RSM solves equation (1) through its model, $D_{T,ij}$ is modelled by Ansys Fluent using an equation of scalar turbulent diffusivity. The equation is given as:

$$D_{T,ij} = \frac{\partial}{\partial x_k}\left(\frac{\mu_t}{\sigma_k}\frac{\partial \overline{u'_\iota u'_J}}{\partial x_k}\right) \quad (5)$$

where σ_k = 0.82 and the turbulent viscosity, μ_t is calculated using the exact formula used in the k-ε model:

$$\mu_t = \rho C_\mu \frac{k^2}{\varepsilon} \quad (6)$$

where $C_\mu = 0.09$, note that this constant used in RSM does not equal to the value used for k-ε models.

Pressure-Strain, ϕ_{ij}

In Ansys Fluent, the pressure-strain term is calculated and modelled automatically by the governing equation:

$$\phi_{ij} = \phi_{ij,1} + \phi_{ij,2} + \phi_{ij,w} \quad (7)$$

where $\phi_{ij,1}$, $\phi_{ij,2}$ and $\phi_{ij,w}$ are the slow pressure-strain term, rapid pressure-strain term and wall reflection term respectively.

RSM approaches the slow pressure-strain term, $\phi_{ij,1}$ by default using the equation:

$$\phi_{ij,1} = -C_1 \rho \frac{\varepsilon}{k}\left(\overline{u'_\iota u'_J} - \frac{2}{3}\delta_{ij}k\right) \quad (8)$$

where C_1 is constant 1.8.

On the other hand, the rapid pressure-strain term, $\phi_{ij,2}$ is modelled by the equation:

$$\phi_{ij,2} = -C_2\left[\left(P_{ij} + F_{ij} + \frac{5}{6}G_{ij} - C_{ij}\right) - \frac{2}{3}\delta_{ij}\left(P + \frac{5}{6}G - C\right)\right] \tag{9}$$

where C_2 is 0.6, C is $0.5C_{kk}$ while P_{ij}, F_{ij}, G_{ij} and C_{ij} is as explained in equation (1).

The final term of the pressure-strain term which is the wall reflection term, $\phi_{ij,w}$ is rather complex as it functions to redistribute the normal stresses near the wall. The term is modelled using the equation:

$$\phi_{ij,w} = C'_1\frac{\varepsilon}{k}\left(\overline{u'_k u'_m}\, n_k n_m \delta_{ij} - \frac{3}{2}\overline{u'_i u'_k}\, n_j n_k - \frac{3}{2}\overline{u'_j u'_k}\, n_i n_k\right)\frac{C_l k^{\frac{3}{2}}}{\varepsilon d} + C'_2\left(\phi_{km,2} n_k n_m \delta_{ij} - \frac{3}{2}\phi_{ik,2} n_j n_k - \frac{3}{2}\phi_{jk,2} n_i n_k\right)\frac{C_l k^{\frac{3}{2}}}{\varepsilon d} \tag{10}$$

where C'_1 is 0.5, C'_2 is 0.3, $C_l = C_\mu^{\frac{3}{4}}$ where C_μ is 0.9, k is the von Karman constant with the value of 0.4187 while n_k and d is the $x_k$component of the unit and distance normal to the wall respectively

Buoyancy Production, G_{ij}

The effects of buoyancy modelled in RSM turbulent model is governed by the equations:

$$G_{ij} = -\rho\beta\left(g_i\overline{u'_j\theta} + g_j\overline{u'_i\theta}\right) \tag{11}$$

$$\overline{U_i\theta} = \frac{\mu_t}{Pr_t}\left(\frac{\partial T}{\partial x_i}\right) \tag{12}$$

where the Prandt number, Pr_t =0.85, which is the turbulent number for energy and β stands for the coefficient of thermal expansion which is further elaborated by the equation:

$$\beta = -\frac{1}{\rho}\left(\frac{\partial \rho}{\partial T}\right)_p \tag{13}$$

Solving equation (13) for buoyancy production in ideal gases, the following equation is obtained and modelled for RSM:

$$G_{ij} = -\frac{\mu_t}{Pr_t}\left(g_i\frac{\partial \rho}{\partial x_j} + g_j\frac{\partial \rho}{\partial x_i}\right) \tag{14}$$

Dissipation, ε_{ij}

In RSM, the dissipation rate in a turbulent system is modelled using the equation:

$$\varepsilon_{ij} = \delta_{ij}(\rho\varepsilon + Y_M) \tag{15}$$

where Y_M is the additional dilatation dissipation and ε is the scalar dissipation rate. It can be solved using the following expression:

$$Y_M = 2\rho\varepsilon {M_t}^2 \tag{16}$$

where M_t is defined as the Mach number and can be calculated using the formula:

$$M_t = \sqrt{\frac{k}{a^2}} \tag{17}$$

where a is the speed of sound. The scalar dissipation rate, ε which is present in both equations (15) and (16) is solved using the same transport equation used in the k- ε model. The equation is as follows:

$$\frac{\partial}{\partial t}(\rho\varepsilon) + \frac{\partial}{\partial x_i}(\rho\varepsilon u_i) = \frac{\partial}{\partial x_j}\left[\left(\mu + \frac{\mu_t}{\sigma_\varepsilon}\right)\frac{\partial \varepsilon}{\partial x_j}\right] C_{\varepsilon 1}\frac{1}{2}[P_{ii} + C_{\varepsilon 3}G_{ii}]\frac{\varepsilon}{k} - C_{\varepsilon 2}\rho\frac{\varepsilon^2}{k} + S_\varepsilon \tag{18}$$

where σ_ε , $C_{\varepsilon 1}$ and $C_{\varepsilon 2}$ is 1.0, 1.44 and 1.92 respectively while $C_{\varepsilon 3}$ is computed as a function of local flow direction relative to gravitational vector. S_ε is denoted as user-defined source term.

2.3 Discrete Phase Model

There are two methods in calculating particle laden flows in a fluid using CFD [40]. The methods are the discrete phase model (DPM) and multiphase model. As shown in Table 1, almost all studies involving CFD in cyclone separator design uses the DPM. This is because the second injected phase only constitutes a small percentage of volume; and if the case indicates otherwise, the multiphase model should be used. Hence, the interactions between the particles can be ignored and DPM is used to calculate the interactions of the said particles in the fluid flow. The governing equations of DPM follows the Euler-Langrage approach where the fluid phase is treated as a continuum in solving the Navier-Stokes equations. In DPM, the trajectory of a single particle is governed numerically by equating its inertia to the forces acting on it. The equation is given as the following:

$$\frac{d\overrightarrow{u_p}}{dt} = F_D(\underset{u}{\rightarrow} - \underset{u_p}{\rightarrow}) + \frac{\vec{g}(\rho_p - \rho)}{\rho_p} + \underset{F}{\rightarrow} \tag{19}$$

where $\underset{u}{\rightarrow}$ = fluid phase velocity, $\underset{u_p}{\rightarrow}$ = particle velocity, μ = molecular velocity of the fluid, ρ = density of fluid, ρ_p = density of particle, $\underset{F}{\rightarrow}$ = additional acceleration, force per unit particle mass and $F_D(\underset{u}{\rightarrow} - \underset{u_p}{\rightarrow})$ = drag force per unit particle mass which can be further elaborated by the equation:

$$F_D = \frac{18\mu\, C_D Re}{\rho_p {d_p}^2\, 24} \tag{20}$$

where d_p = particle diameter and Re, the Reynolds number can be represented by the formula:

$$Re = \frac{\rho d_p|\overrightarrow{u_p} - \vec{u}|}{\mu} \tag{21}$$

while C_D, the drag coefficient from equation (20) is given by the formula, for spherical drag:

$$C_D = a_1 + \frac{a_2}{Re} + \frac{a_3}{Re^2} \tag{22}$$

where a_1, a_2 and a_3 are constants given by Morsi & Alexander (1972).

2.4 Numerical Model Validation

Validation is defined as the process of determining the accuracy of a numerical model to reality [41]. The main purpose of validating a data is the estimation of a range within which the numerical model error lies. This can be achieved by comparing the numerical model findings to the experimental data within specified validation boundaries. In the present study, the numerical model is validated by comparing the pressure drop, axial velocities, u and tangential velocities, v with experimental findings [39]. For this specific goal, the cyclone geometry of Hoekstra's work was replicated to determine the extent of accuracy the numerical model offers for subsequent works in developing an oil palm loose fruit collector. Pressure drop validation was performed by simulating the numerical model at velocities of 5, 7, 9, 10, 15, 18 and 20 ms^{-1}. Pressure profiles and plots of the numerical study were then studied. On the other hand, in determining the accuracy of flow predictions to the turbulent model where RSM is used to simulate the model using the specified boundary conditions, the tangential and axial velocity was plotted along the radial axis at a height of 0.75D from the cyclone separator's bottom exit point at inlet velocity, U_i of 10 m/s.

2.5 Cyclone geometry

The type of cyclone separator is an important design consideration as the swirl in the cyclone will affect their collection performance due to the difference in flow characteristics. In this study, several types of cyclone separator has been considered; 1D2D, 2D2D, and 1D3D cyclone separators. El-Emam *et al*., [6] investigated the performance of various cyclone separators and discovered that the 1D2D cyclone is the most effective among conventional cyclones. The first 'D' indicates the cyclone critical diameter, D_c while the second 'D' refers to the cyclone height in reference to D_c. A 1D2D cyclone separator will have a cyclone height double than that of D_c. Figure 1 provides a standard cyclone with its denoted parts.

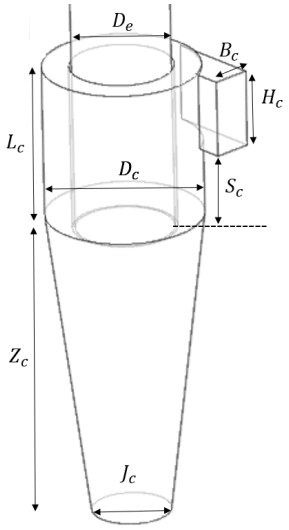

Figure 1. Standard cyclone separator

For data validation purposes, the study will numerically simulate the cyclone geometry of [39] where in their study, the Laser Doppler Anemometry (LDA) method and differential pressure sensors have been adopted to measure the internal velocities and pressure drop of the cyclone separator respectively.

Table 2. Dimensions of designed cyclone

Cyclone part	Dimensions (mm)
D_c	290
B_c	58
D_e	145
H_c	145
J_c	108
S_c	145
L_c	435
Z_c	725

Table 2 gives the measurement of the simulated cyclone separator for data validation. On another note, the cyclone diameter, D_c measured by Hoekstra experimentally differs only by a slight margin of 10 mm compared to the calculated D_c for oil palm loose fruit collections. Hence, the data from the validation process can be studied extensively in designing an efficient loose fruit collector.

2.6 Boundary Condition

Numerous inlet velocities of 5, 7, 15 and 20 ms^{-1} was used for pressure drop validation while an inlet velocity 10 $ms^{-1}$of is used in validating tangential and axial velocity. RSM was used to simulate the cyclone flow field. Wall was set to a no slip condition with standard wall functions. Hydraulic diameter of the gas outlet is B_c=0.58 mm. Hydraulic diameter of the particle's outlet are J_c=108 mm. Turbulence intensity at the gas and particles outlet are specified at 5%. Table 3 shows the solver settings used in the study.

Table 3. CFD solver settings used in the study

Setting	Option/ Input

General	
Gravity	9.81 m s-^{2}
Solver	Pressure based
Velocity formulation	Absolute
Time	Steady
Solution Methods	
Pressure-velocity coupling	SIMPLE
Spatial discretization (Pressure)	Second order
Spatial discretization (Momentum)	Second order upwind
Spatial discretization (Turbulent Kinetic Energy)	Second order upwind
Spatial discretization (Turbulent dissipation Energy)	Second order upwind
Spatial discretization (Energy)	Second order upwind

2.7 Oil Palm Loose Fruit Collector

Upon data validation, the results will then be incorporated in the following simulations. An oil palm loose fruit collector was designed and simulated using the exact CFD settings from Table 3 since the numerical model was validated. According to Wang, [4] the equation to calculate the critical diameter, D_c of a cyclone separator is based on the air flow velocity and flowrate. The equation is given by:

$$D_c = \sqrt{\frac{8Q}{V_i}} \tag{23}$$

where Q is air flow rate (m^3) and V_i is inlet velocity (ms^{-1})

Ramdhan *et al*., [42] stated that the range of air velocity and air flow for loose fruits collecting are 20 - 40 ms^{-1} and 0.28 – 0.33 m^3 respectively. Using the data in Equation 23, a critical diameter, D_c, of 300 mm is obtained. The second larger cyclone separator is meant to trap more materials by having a higher pressure drop. For the second cyclone separator, D_c of 400 mm is chosen. Table 4 displays the parameters of the designed cyclone separator in relation to Figure 1. The designed cyclone separator is depicted in Figure 2.

Table 4. Dimensions of designed cyclone

Dimensions	First cyclone separator (mm)	Second cyclone separator (mm)
D_c	300	400
B_c	75	100
D_e	187.5	250
H_c	150	200
J_c	150	200
S_c	187.5	250
L_c	300	400
Z_c	600	800

Figure 2 depicts the design of a two-stage cyclone separator used in the study. Debris will be introduced into the smaller first stage cyclone separator as the loose fruits are collected via air suction through the inlet. Heavy loose fruits will be gathered via the outlet in the first stage cyclone separator, while lighter debris will be pulled through the vortex finder and collected in the second stage cyclone separator. Clean loose fruits will thus be collected by the first stage cyclone, while undesirable debris would be deposited in the second cyclone.

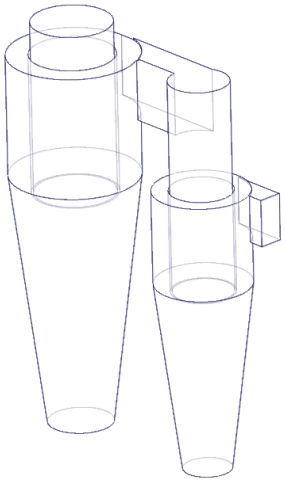

Figure 2. Cyclone separator design used in study

2.8 Boundary Condition and Mesh Generation

An inlet velocity of 20 ms^{-1} was used in the study as it was the lowest setting for an oil palm loose fruit collector suggested by Ahmad *et al*., [43]. RSM and DPM was used to simulate the cyclone flow field and loose fruit collection. Wall was set to a no slip condition with standard wall functions. Hydraulic diameter of the gas outlet is B_c=0.1 m. Hydraulic diameters of the particle's outlet are J_c=0.15 m and 0.2 m respectively. Turbulence intensity at the gas and particles outlet are specified at 5%. For the discrete phase model (DPM), an injection with density 995.7 kg/m^3 and 0.04 m was set to simulate oil palm loose fruit collection into the system [44].

Table 4.Details of every mesh level used in the grid independence study

Simulation	1	2	3	4	5	6	7
Element size (m)	0.02	0.0175	0.015	0.0125	0.01	0.0075	0.005
Elements (n)	137140	194739	279143	444266	769907	1492227	3993332

A total of 7 levels of mesh are created by decreasing the element size by 0.0025 m for each level, starting with an element size of 0.02 m. As demonstrated in Table 4, as the element size is reduced, the number of cells grows for each level. In order to investigate the simulation accuracy and computing costs, the identical solver settings are applied to all seven meshes. This phase is critical in determining the best mesh size for subsequent works. It is worth noting that the solution is mesh-independent when the error derived from the results does not change considerably while increasing the number of cells in an attempt to improve simulation accuracy. It is also critical that the chosen mesh size achieves accurate simulation results while not using a significant amount of simulation time in order to reduce computing costs. Mesh level 5 was subsequently selected at 769907 elements a shown in Figure 3.

3.0 RESULTS AND DISCUSSION

3.1 Pressure Drop

Pressure drop validation was performed by simulating the numerical model at velocities of 5, 7, 10, 15 and 20 $\boldsymbol{ms^{-1}}$. This step ensures the solver settings in the numerical study behaves accurately and demonstrates reliable precision. Figure 4 shows a comparison of the numerical simulation to experimental work where the pressure drops were measured across varied inlet velocity using pressure differential sensors. As can be seen, the simulated data is in good agreement with experimental data where maximum percentage difference compared to experimental data were recorded at 7.5% while the minimum was 0.4 %. Note that the percentage difference is obtained by calculating the difference of simulated data to experimental data. Verily, precisely close comparisons of the numerical study data with the works of Hoekstra are indications that the present work is consistent and of reasonable precision.

Figure 3. Mesh of cyclone separators with 769907 elements

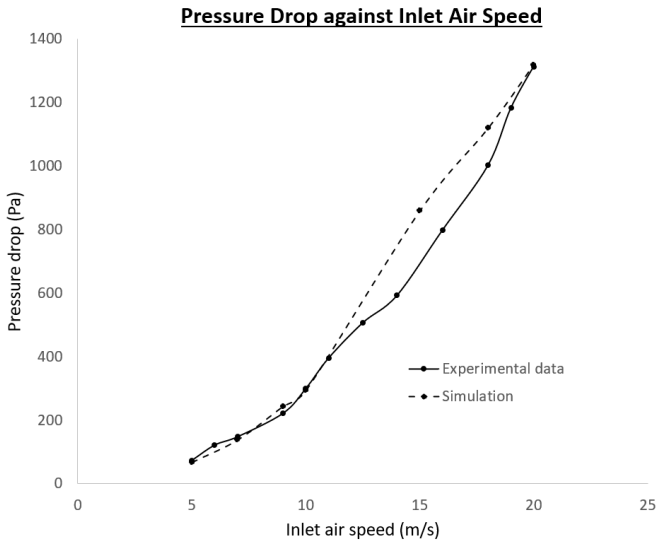

Figure 4. Pressure drop comparison between numerical simulation and experimental data

In general, pressure drop in a cyclone separator is attributed to the kinetic energy losses, frictional losses in the outer vortex, cyclone entry exit losses, pressure losses in the inner vortex and exit point. All of which are directly affected by the cyclone's inlet velocity. Hence, it can be seen that the graph showed in Figure 4 depicted a nearly direct proportionality trend between inlet air speed and pressure drop. For a more comprehensive analysis of the cyclone flow in relation to the pressure drop, the contour plots of the static and total pressure are studied. The working principle of a cyclone separator is to collect heavy materials while the lighter debris are sucked out of the system. Thus, pressure considerations dictate that there must be a negative pressure along the central axis of the cyclone. The presence of negative pressure indicates the presence of a vacuum suction, which eliminates lighter particles from the collected materials. The vertical and horizontal pressure contours for the cyclone separator are shown in Figure 5. As can be observed, there are negative pressure segments, shown in dark blue that run along the central axis of the cyclone separator. This is consistent theoretically where the cyclone separator will act as intended by sucking light materials and debris out of the system via air suction along the central axis. The pressure contours exhibited satisfactory patterns to confirm the presence of a Rankine vortex flow, which consists of a free vortex swirl along the external region with an inner vortex present at the core vertically [22]. However, the pressure contours alone, cannot fully represent the actual flow in confirming the presence of a Rankine flow. To visualize the flow of the studied cyclone separator more accurately, velocity profiles of the cyclone separator are studied.

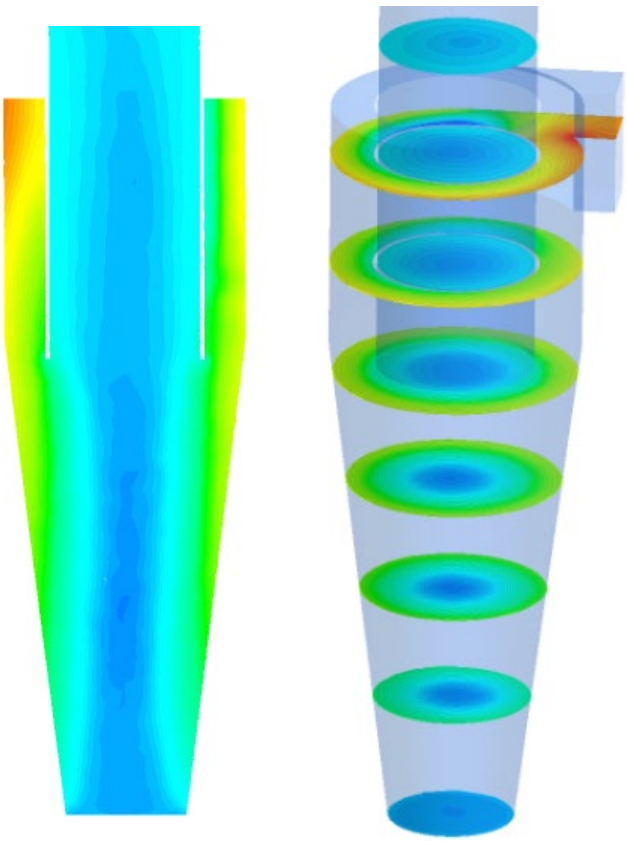

Figure 5 (a) and (b). Vertical and horizontal pressure contours

3.2 Tangential Velocity

Tangential velocity is an imperative indication of a cyclone separator performance. The effects of the tangential velocity variations in the cyclone flow will then generate the centrifugal force responsible in material separation where particles will be pushed to the walls and lighter materials will move towards the cyclone center. In Figure 6, it can be seen that the experimental data by Hoekstra [39], and the simulated data from the present study exhibited the same pattern with minor deviations. The maximum error recorded was 14.98% in the profile at radial position of 0.58. However, for other regions the errors were very minimal and this showed that the numerical simulation obeys the cyclone separator mechanism as validated by experimental data. Furthermore, tangential velocity trend indicates that the cyclone behaves theoretically with the presence of swirling along the tangential axis. The same trend of opposing directions is exhibited at different directions from the centre radius where the velocity slowly increases to a maximum and declines near the cyclone wall. Theoretically, a swirl is proven to exist in the cyclone separator.

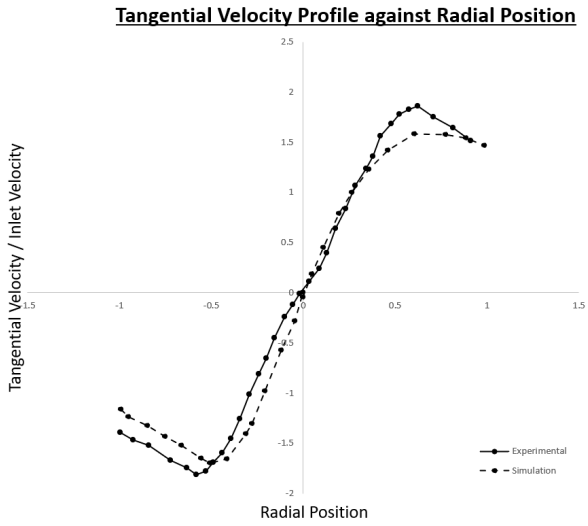

Figure 6. Tangential velocity comparison between numerical simulation and experimental data.

It has been observed that a swirling flow has been confirmed through the tangential velocity trends and a negative suction region is confirmed through the pressure trends. However, the directions of vertical flow have yet to be confirmed. Thus, an analysis on axial velocity in the cyclone separator is paramount to prove the theoretical behaviour.

3.3 Axial Velocity

From Figure 7, it is evident that the numerical simulation is in good agreement with the experimental data at a satisfactory level. The plotted curve depicts an 'M' shape which shows the simulation behaves as intended compared to experimental data. The axial velocity records a negative velocity on both ends of the cyclone diameter, slowly increasing in axial velocity towards the centre, then plunges to an almost 0 velocity at the central axis. This is proof a central vortex, the Rankine flow exists. This phenomenon indicates that the flow near the wall brings materials down, while an upward trend with maximum velocity is seen swirling along the central axis where a slow-moving centre is observed. Figure 8 shows the velocity contour in the vertical direction. It can be observed that a green positive region further supported the presence of a Rankine flow which carries debris out of the cyclone separator while the regions along the walls carries materials towards the cyclone exit below.

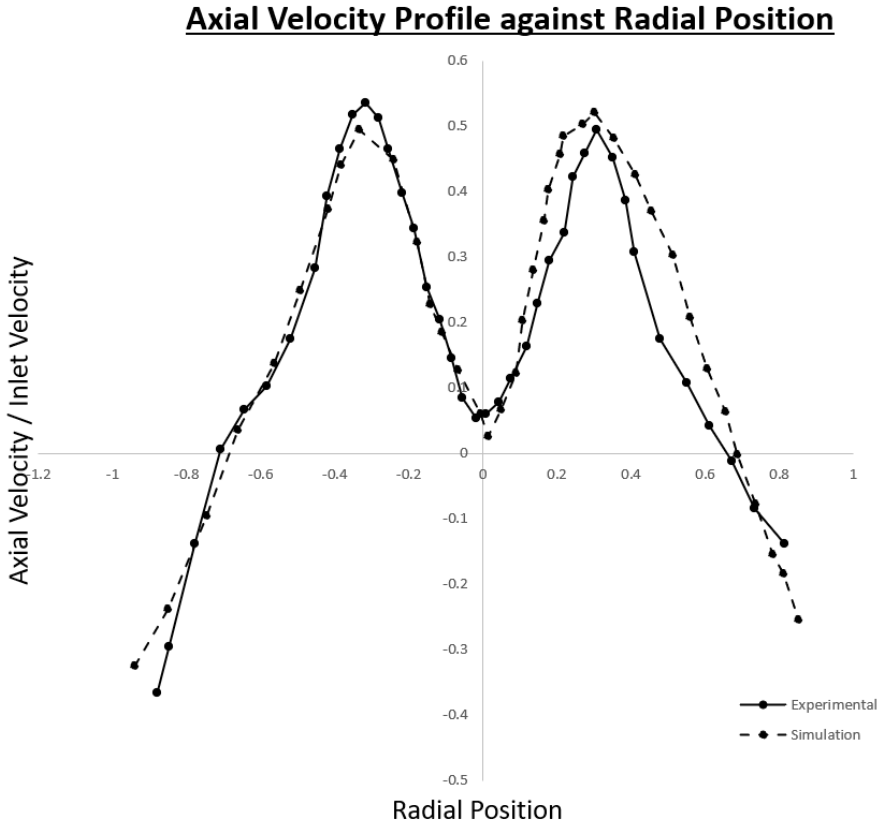

Figure 7. Axial velocity comparison between numerical simulation and experimental data.

3.4 Further Investigation of Oil Palm Loose Fruit Collector

An oil palm loose fruit collector which targets to filter out unwanted debris was proposed. Figure 5 shows horizontal cross section pressure trends in the simulated oil palm loose fruit collector. Horizontal pressure cross sections reveal a downward pressure trend from the cyclone wall to the cyclone centre. The system is behaving as expected, with debris being dragged along with air from particles spinning around the walls towards the cyclone core. The contours and vectors exhibited satisfactorily confirm the presence of a Rankine vortex flow, which consists of a free vortex swirl along the external region with an inner vortex present at the core vertically. A satisfactory collection efficiency is recorded from the DPM study at 83.06% where it was calculated by calculating the percentage of fruits being collected by particles compared to the fruits injected in the system. However, through further study it was found that using a square vortex finder as depicted in Figure 9 is favourable to the system where a collection efficiency of 92.82 % was recorded at the same inlet velocity.

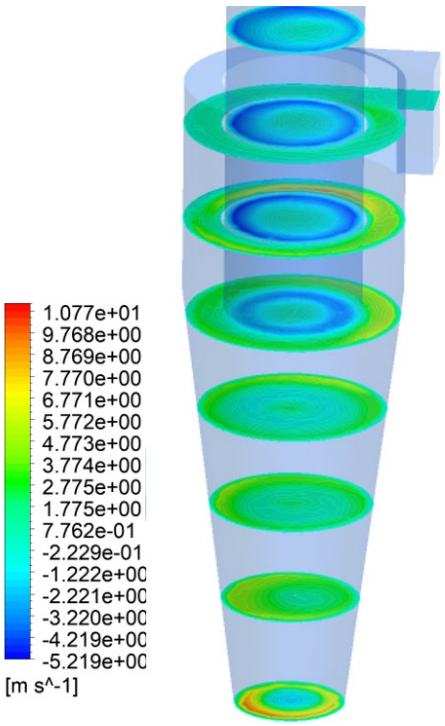

Figure 8. Z-velocity cross section contour

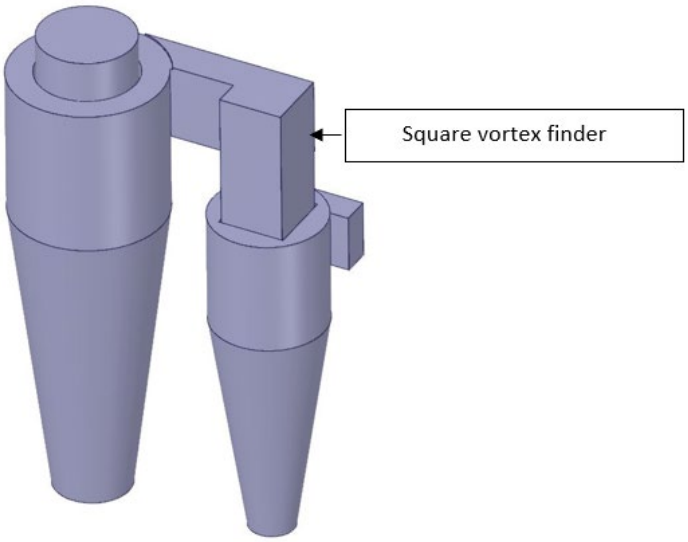

Figure 9. Newly developed system with square vortex finder

To further visuallize the system of a square vortex finder cyclone separator, the velocity magnitude and x-velocity plots from the bottom quarter of the separator are observed in Figure 10 and 11. From Figure 10, the graph observes to slowly step up until a maximum, staying almost constant with slight decrease along the central axis and increases back to a minimum where it will decrease steeply to a minimum. This occurrence confirms the absence of a Rankine flow as mentioned earlier as the characteristic if a Rankine flow constitutes of a stagnation point with almost zero velocity along the central axis as discussed in the previous sections and verified in Figures 5 and 8. The velocity magnitude in Figure 10 does decrease slightly along the central axis indicating of a suction, but it is not categorized as a Rankine flow due the significant magnitude recorded. Next, from Figure 11 it can be seen that the x-velocity plot depicts an inverted sine-graph shape. The phenomenon showed here is of interest due the fact that despite the absence of a Rankine flow, a swirling flow along the walls of the cyclone separator is present. Hence, it can be deduced that the material sucked into the system will swirl along the cyclone separator's inner walls to be collected. However, since a Rankine flow is not present the central axis of the cyclone separator will experience a direct suction flow as opposed to a reverse cyclone suction flow present in Rankine flows.

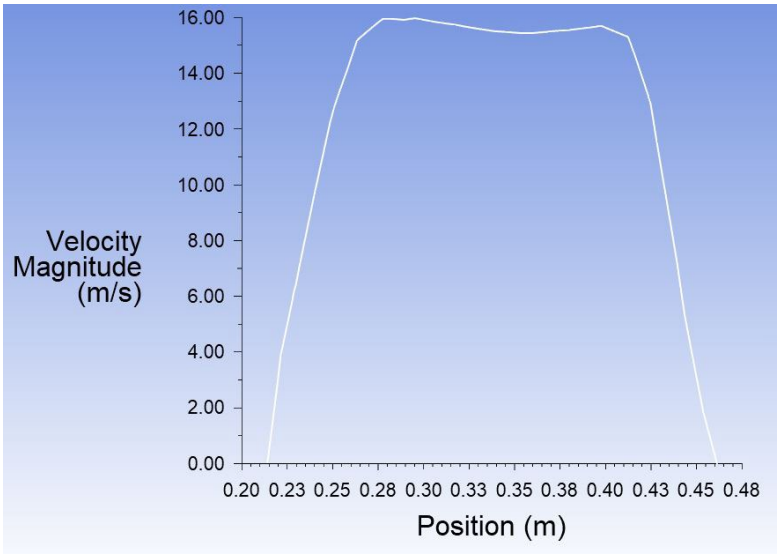

Figure 10. Velocity magnitude plot

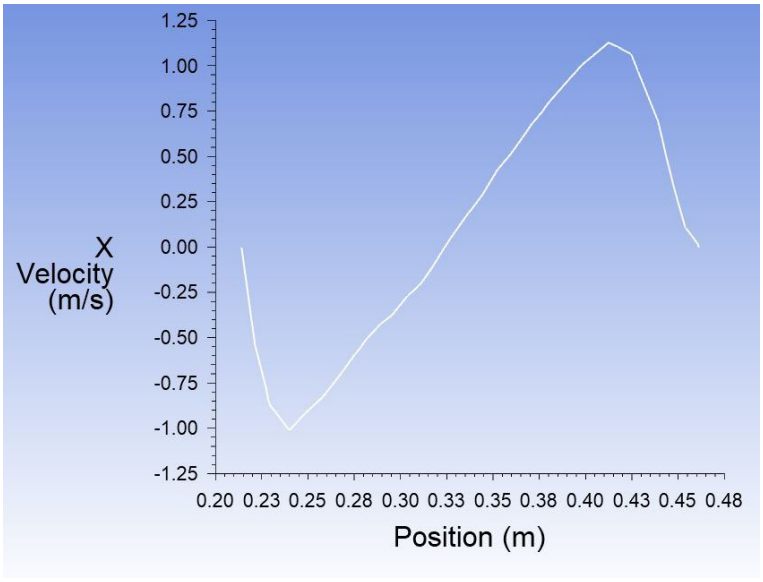

Figure 11. X- Velocity plot

4.0 CONCLUSION

Results have showed that the numerical study employing RSM was in good agreement with theory in terms of cyclone flow. Analysis of cyclone separator's flow field in terms of static pressure, total pressure, axial velocity, and tangential velocity have confirmed that the model behaved in accordance with theory by demonstrating presence of Rankine vortex. Results have provided the necessary code verification technical data cyclone separator operation which will be used for oil palm loose fruit collections where CFD data was scarce. Preliminary work on simulating an oil palm loose fruit collector is satisfactory with a dominant Rankine vortex flow with an efficient collection of 83.06%. In developing an efficient oil palm loose fruit collector, it was found that using a square vortex finder is favourable where a 92.82% collection efficiency was recorded. It also worth noting that further experimental works are also essential in validating the findings and other issues such as the means of transports in estates and the evacuation methods of the loose fruits out of the estates must also come into account for practical usage of the developed system.

5.0 CONFLICT OF INTEREST

The authors declare no conflicts of interest.

6.0 ACKNOWLEDGEMENT

This work was supported by Universiti Teknologi Malaysia (UTM) under the UTM-Matching Grant (Grant Number: Q.J130000.3024.04M81).

7.0 REFERENCES

[1] Khalid, M. R. & Shuib, A. R. (2017). Performance of oil palm loose fruits separating machine. Journal of Oil Palm Research. Vol. 29 (3). pp. 358-365. https://doi.org/10.21894/jopr.2017.2903.08

[2] Shuib, A.R., Khalid, M.R., Deraman, M.S. & Mohamed, A. (2012). Oil Palm Loose Fruit Collector No.505, MPOB Information Series No.57, Malaysia Palm Oil Board (MPOB), Selangor.

[3] Park, D. & Go, J. (2020). Design of Cyclone Separator Critical Diameter Model Based on Machine Learning and CFD. Processes. 8. 10.3390/pr8111521.

[4] Wang, L. 2004, Theoretical study of cyclone design, Doctoral Thesis, Texas A&M University.

[5] Safikhani, H., Akhavan-Behabadi, M. A., Shams, M. & Rahimyan, M.H. (2010). Numerical simulation of flow field in three types of standard cyclone separators. Advanced Powder Technology. Volume 21. Issue 4. pp. 435-442,

[6] El-Emam, M. A., Zhou, L., Shi, W. & Han, C. (2021). Performance evaluation of standard cyclone separators by using CFD–DEM simulation with realistic bio-particulate matter. Powder Technology. Volume 385. pp. 357-374. https://doi.org/10.1016/j.powtec.2021.03.006

[7] Fu, S., Zhou, F., Sun, G., Yuan, H. & Zhu, J. (2021). Performance evaluation of industrial large-scale cyclone separator with novel vortex finder. Advanced Powder Technology. 32. pp. 931–939. https://doi.org/10.1016/j.apt.2021.01.033

[8] Wasilewski, M., Brar, L. & Ligus, G. (2020). Experimental and numerical investigation on the performance of square cyclones with different vortex finder configurations. Separation and Purification Technology. 239. 116588

[9] Sakin, A., Karagov, I. & Avci., A. (2019). Performance analysis of axial and reverse flow cyclone separators. Chemical Engineering and Processing - Process Intensification. Volume 144. https://doi.org/10.1016/j.cep.2019.107630.

[10] Parvaz, F., Hosseini, S. H., Elsayed, K. & Ahmadi, G. (2018). Numerical investigation of effects of inner cone on flow field, performance and erosion rate of cyclone separators. Separation and Purification Technology. 201. pp. 223-237.

[11] Wei, Q., Sun, G. Gao, C. (2020). Numerical analysis of axial gas flow in cyclone separators with different vortex finder diameters and inlet dimensions. Powder Technology. Volume 369. pp. 321-333. https://doi.org/10.1016/j.powtec.2020.05.038

[12] Kumar, V. Jha, K. (2019). Multi-objective shape optimization of vortex finders in cyclone separators using response surface methodology and genetic algorithms. Separation and Purification Technology. Volume 215, pp. 25-31. https://doi.org/10.1016/j.seppur.2018.12.083

[13] Elsayed, K. & Lacor, C. (2013). The effect of cyclone vortex finder dimensions on the flow pattern and performance using LES. Computers & Fluids. Volume 71. pp.224-239. https://doi.org/10.1016/j.compfluid.2012.09.027

[14] El-Batsh. H. M. (2013). Improving cyclone performance by proper selection of the exit pipe. Applied Mathematical Modelling. Volume 37. Issue 7. pp. 5286-5303. https://doi.org/10.1016/j.apm.2012.10.044

[15] Yao, Y., Shang, M., Ke, X., Zhang, J., Huang, Z, Zhou, T., & Lyu. J. (2024). Design of multi-stage contracted inlet duct for cyclone separators, Separation and Purification Technology. Volume 332. 125753. https://doi.org/10.1016/j.seppur.2023.125753.

[16] Surahmanto, F., Pamungkas, A., Dhimas, A. M., Soemawidagdo, A. L., Sasongko, B. T., Sukardi, S., Lutfianto, R. & Pratama Hakim, M. R. (2024). Performance Evaluation of Square Cyclones Separator with Cone Geometry Variations. CFD Letters. Volume 16. No. 7:July. https://doi.org/10.37934/cfdl.16.7.136149.

[17] Babaoğlu, N. & Parvaz, F., Hosseini, S. H., Elsayed, K. & Ahmadi, G. (2021). Influence of the inlet cross-sectional shape on the performance of a multi-inlet gas cyclone. Powder Technology. 384. pp. 82-99.

[18] Yu, G., Dong, S., Yang, L., Yan, D., Dong, K., Wei, Y. & Wang, B. (2021). Experimental and numerical studies on a new double-stage tandem nesting cyclone. Chemical Engineering Science. Volume 236. 116537.

[19] Gao, Z. & Wang, J., Liu, Z., Wei, Y., Wang, J. & Mao, Y. (2020). Effects of different inlet structures on the flow field of cyclone separators. Powder Technology. 372. pp. 519-531.

[20] Misiulia, D. & Antonyuk, S., Andersson, A., Lundström, T. (2020). High-efficiency industrial cyclone separator: A CFD study. Powder Technology. 364. pp. 943-953.

[21] Qiang, L., Wang, J. Xu, W. & Meng, Z. (2020). Investigation on separation performance and structural optimization of a two-stage series cyclone using CPFD and RSM, Advanced Powder Technology, Volume 31, Issue 9, pp. 3706-3714.

[22] Shastri, R. & Brar, L. (2020). Numerical investigations of the flow-field inside cyclone separators with different cylinder-to-cone ratios using large-eddy simulation. Separation and Purification Technology. 249. 117149. https://doi.org/10.1016/j.seppur.2020.117149

[23] Nassaj, O. R., Toghraie, D. & Afrand, M. (2019). Effects of multi inlet guide channels on the performance of a cyclone separator. Powder Technology. Volume 356. pp. 353-372.

[24] Erol, H.I., Turgut, O. & Unal, R. Experimental and numerical study of Stairmand cyclone separators: a comparison of the results of small-scale and large-scale cyclones. Heat Mass Transfer 55, 2341–2354 (2019). https://doi.org/10.1007/s00231-019-02589-y

[25] Yohana, E., Tauviqirrahman, M., Putra, A. R., Ade, E. D. & Choi, K. H. (2018). Numerical analysis on the effect of the vortex finder diameter and the length of vortex limiter on the flow field and particle collection in a new cyclone separator. Cogent Engineering. 5:1. 1562319

[26] Siadaty, M., Kheradmand, S. & Ghadiri, F. (2017). Study of inlet temperature effect on single and double inlets cyclone performance. Advanced Powder Technology. Volume 28. Issue 6. pp. 1459-1473.

[27] Misiulia, D., Andersson, A. & Lundström, T. (2017). Effects of the inlet angle on the collection efficiency of a cyclone with helical-roof inlet. Powder Technology. 305. pp. 48-55.

[28] Hamdy, O., Bassily, M. A., El-Batsh, H. M. & Mekhail, T. M. (2017) Numerical study of the effect of changing the cyclone cone length on the gas flow field, Applied Mathematical Modelling. Volume 46. pp. 81-97.

[29] Wasilewski, M. & Duda, J. (2016). Multicriteria optimisation of first-stage cyclones in the clinker burning system by means of numerical modelling and experimental research. Powder Technology. 289. pp. 143-158.

[30] Misiulia, D., Andersson, A. & Lundström, T. (2015). Effects of the inlet angle on the flow pattern and pressure drop of a cyclone with helical-roof inlet. Chemical Engineering Research and Design. Volume 102. pp.307-321.

[31] Li H., Gao B. &Li B., (2015). Numerical Analysis of Flow Dynamics of Cyclone Separator Used for Circulating Fluidized Bed Boiler. Chemical Engineering Transactions, 46.pp.991-996.

[32] Souza, F. J., Salvo, R. V. & Martins, D. M. (2015). Effects of the gas outlet duct length and shape on the performance of cyclone separators. Separation and Purification Technology. Volume 142. pp. 90-100.

[33] Hui Ci, H. & Sun, G. (2015). Effects of Wall Roughness on the Flow Field and Vortex Length of Cyclone. Procedia Engineering. Volume 102. pp. 1316-1325. https://doi.org/10.1016/j.proeng.2015.01.262.

[34] Brar, L., Sharma, R., & Elsayed, K. (2015). The Effect of the Cyclone Length on the Performance of Stairmand High-Efficiency Cyclone. Powder Technology. 286. pp. 668-677.

[35] Elsayed, K. & Lacor, C. (2012). The effect of the dust outlet geometry on the performance and hydrodynamics of gas cyclones. Computers & Fluids. Volume 68. pp. 134-147.

[36] Elsayed, K. & Lacor, C. (2011). The effect of cyclone inlet dimensions on the flow pattern and performance. Applied Mathematical Modelling. Volume 35, Issue 4. pp. 1952-1968.

[37] Elsayed, K. & Lacor, C. (2010). The effect of vortex finder diameter on cyclone separator performance and flow field. V European Conference on Computational Fluid Dynamics. 14-17 June 2010.

[38] Gimbun, J., Chuah, L. A., Choong, T. S. Y. & Fakhru'l-Razi, A. (2005). Prediction of the effects of cone tip diameter on the cyclone performance. Journal of Aerosol Science. 36. pp. 1056-1065.

[39] Hoekstra, AJ., Derksen, JJ., & Van Den Akker, HEA. (1999). An experimental and numerical study of turbulent swirling flow in gas cyclones. Chemical Engineering Science, 54(13-14), pp. 2055-2065.

[40] ANSYS FLUENT Theory Guide, ANSYS, Inc., Release 15.0, November 2013.

[41] Standard for Verification and Validation in Computational Fluid Dynamics and Heat Transfer, The American Society of Mechanical Engineers., R2021, 2009.

[42] Ramdhan, M. K., Rahim, A. S. & Norman, K. (2019). Determination of minimum suction level of collecting oil palm loose fruits. Konvensyen Kebangsaan Kejuruteraan Pertanian dan Makan 2019, Putrajaya. pp. 198-201.

[43] Ahmad, H., Ahmad Zamri, M.Y, & Mohd S. J. (1995). Loose Fruit Collector. PORIM Information Series No.19, Palm Oil Research Institute of Malaysia (PORIM), Selangor.

[44] Owolarafe, O.K., Olabige., M. T., & Faborode., M. O. (2007). Physical and mechanical properties of two varieties of fresh oil palm fruit. Journal of Food Engineering. Volume 78. Issue 4. pp. 1228-1232. https://doi.org/10.1016/j.jfoodeng.2005.12.049